

## Supporting Information

### Ciliated micropillars for the microfluidic-based isolation of nanoscale lipid vesicles

5 Zongxing Wang<sup>a,b</sup>, Hung-jen Wu<sup>a</sup>, Daniel Fine<sup>a</sup>, Jeffrey Schmulen<sup>a</sup>, Ye Hu<sup>a</sup>, Biana Godin<sup>a</sup>, John X. J. Zhang<sup>\*b</sup>,  
Xuewu Liu<sup>\*a</sup>

**Reverse pulse silver deposition on the sidewalls of micropillars.** Silver nanopattern determines the distribution of porous silicon nanowires, thus determines the inter-nanowire spacing between nanowires. Uniform silver nanopattern is highly  
10 desired in order to achieve consistent trapping of target nanoparticles. Previously reported electroless deposition would result in non-uniform silver coverage along the vertical direction due to the surface irregularities of tall micropillars. To deposit uniform silver nanopattern on micropillars, the pulse reverse electroplating method was adapted. The experimental set-up for pulse reverse electroplating is shown in Figure S1. Silicon wafer with micropillars is cleaned in the Piranha solution then dipped in HF solution to remove native oxide. The wafer is assembled in the Teflon electroplating cell, and  
15 sealed with a Viton O-ring. Aluminum foil is used as backside contact. A platinum mesh is immersed in 0.5 M AgNO<sub>3</sub> plating solution as electrode. A waveform generator is used to control the reverse pulse parameters including voltage, duty cycle and time. Depending on the feature size and aspect ratio of the micropillars, the pulse parameters are tuned accordingly to optimize the silver pattern based on SEM monitoring.

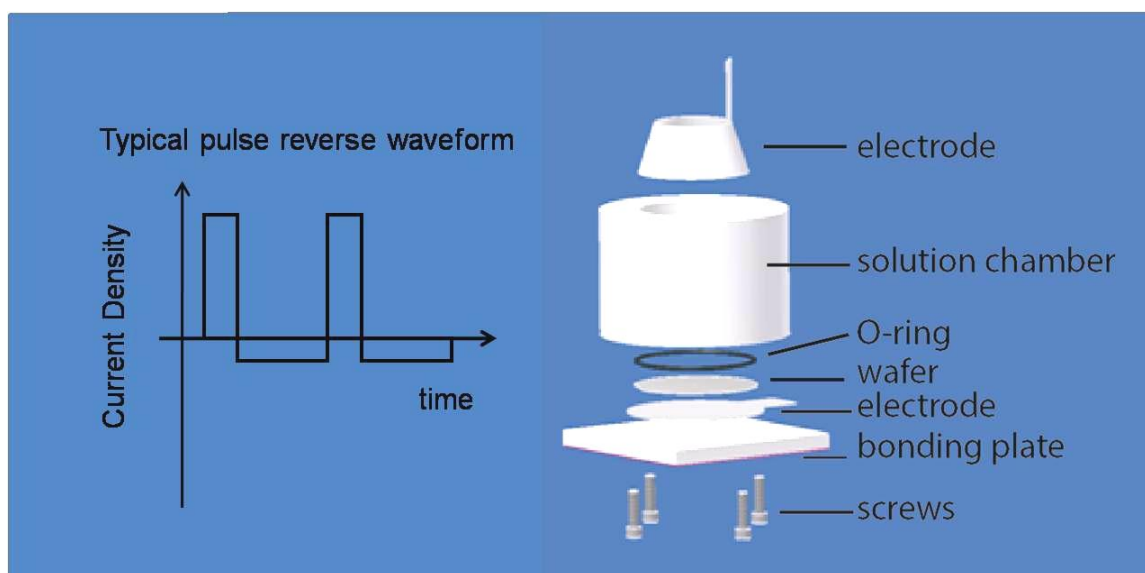
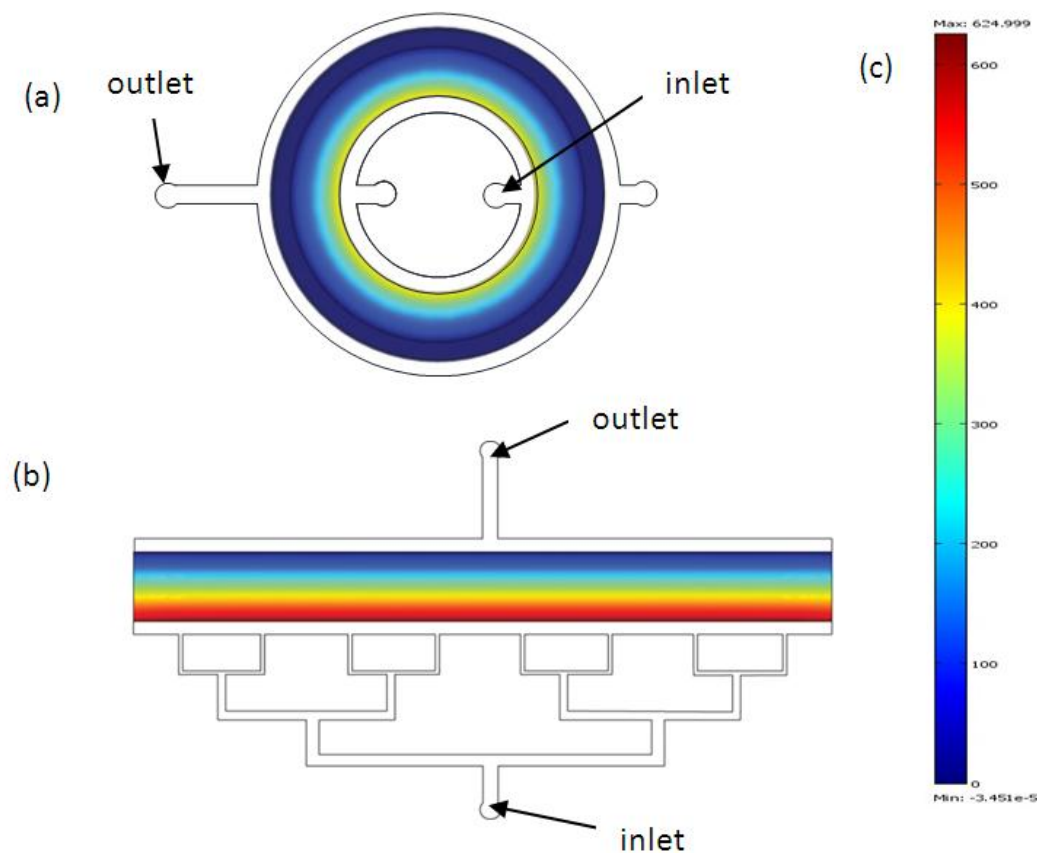


Figure S1. Representative pulse reverse waveform and electroplating cell assembly

**Flow resistance in microfluidic channels with micropillars.** Several factors of the nanowire-on-pillar structure are essential for efficiently harvesting exosomes: the density of micropillars, the height of micropillars, and the morphology of the nanowires. Higher density of micropillars and longer nanowires provide more binding sites for exosomes, but increase  
25 the flow resistance. In our devices, the distances between pillars are 900nm in order to filter large cells naturally occurring in biological fluids. A hexagonal arrangement of micropillars with 2.6  $\mu\text{m}$  in diameter was adapted (Main text Figure 3a) for high density packing in order to achieve a higher binding site density and to increase the possibility of capturing exosomes. High density arrays of micropillars will cause very high hydrodynamic resistance in the assembled microfluidic devices. A rational designed microfluidic channel with micropillars will be very beneficial to increase the reliability and  
30 efficiency of the device. We simulated the pressure drop across two different channel configurations, a concentric radial-flow channel and a straight channel, as shown in Figure S2. The simulation was done using Comsol 4.3 free and porous media flow model, and only micropillar region was simulated. In these two layouts, the area of entry port is kept the same, and the distance of particle traveling of both the circular channel design and straight channel design are also kept the same. As a result, the pressure drop across the pillar array in the radial-flow channel is reduced by 30% compared to that in the

straight channel when injecting sample at the same rate. The reason for this reduced pressure drop effect is lower average flow speed in circular design than square design due to flow front expansion at larger diameter. Based on this calculation, a concentric radial-flow microfluidic device was designed with 4mm flow path.



5 Figure S2. Comsol simulation of pressure drop across micropillar arrays in two channel designs with the same entry front area and same travelling distance. (a) Pressure drop in a radial-flow concentric channel. (b) Pressure drop in a straight channel. (c) Pressure scale bar with arbitrary unit.

**Fabrication of ciliated micropillar microfluidic prototypes.** The nanowire-on-micropillar structure was fabricated in two steps. First, arrays of 2.6µm circles are patterned on silicon wafer by photolithography, and followed by the deep silicon etching to generate array of 22µm tall micropillars. The second step is to deposit silver nanopattern on the side-walls of micropillars using reverse pulse electroplating, and form porous silicon nanowires all around the micropillars by metal-assisted electroless etching. The fabrication process flow is shown in Figure S3. In details, a p-type silicon wafer with resistivity 0.005 Ω-cm is cleaned in Piranha and dipped in 5% HF solution for 5 minute to remove surface oxide. An 80 nm thick low stress silicon nitride is deposited on the substrate using LPCVD. Then a 50 nm thick Chromium (Cr) film is deposited on a CHA e-beam evaporator. The Cr film acts as a hard mask for deep silicon etching, and the nitride layer is to protect the top surfaces of micropillars in the nanowire etching step. Fluidic channels with micropillar array are defined by photolithography. The pattern is transferred into mask layer by reactive ion etching. Botch process on an ICP etcher is used to create high aspect ratio micropillar structure as well as the microfluidic channels. Cr mask layer is then removed by wet etching, leaving nitride on the top surfaces of the structure. The wafer with micropillars is dipped in 5% HF solution for 5 minutes to remove native oxide, rinsed with ethanol and dried using blown air. The wafer assembled in an electroplating cell with the micropillar side immersing in the 0.5 M AgNO<sub>3</sub> electrolyte. The reverse pulse electroplating is performed to deposit uniform silver nanopattern on the sidewalls of the micropillars. Then, the wafer is chemically etched in a mixture of 0.1M H<sub>2</sub>O<sub>2</sub>, 2.9M HF solution for 1 minute to create 400 nm long porous silicon nanowires etched into all-around the micropillars. Silver is stripped by immersion in silver etchant (Transene Company) for 2 minutes. A 5 nm layer of silicon

oxide layer is grown on the surface. After a short oxygen plasma treatment, the ciliated micropillar structure is bonded with PDMS to complete the microfluidic prototype.

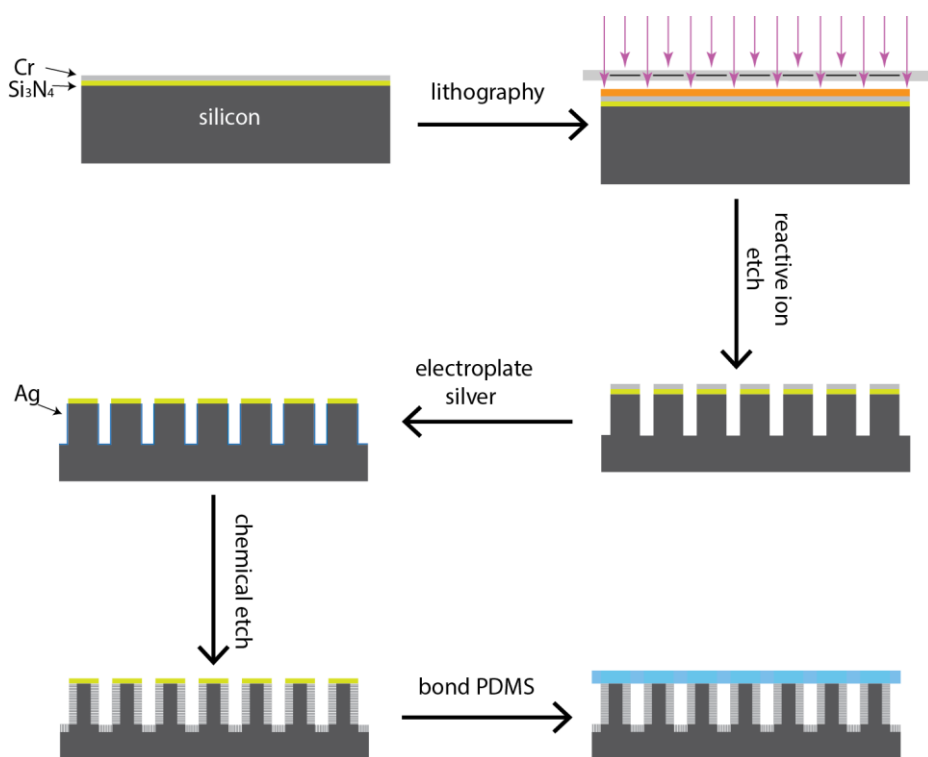


Figure S3. Diagram of the fabrication procedure of microfluidic device with the hierarchical ciliated micropillar structure.

5

**Materials.** AgNO<sub>3</sub> was purchased from Sigma-Aldrich (St. Louis, MO). P-type (100) silicon wafers with resistivity of 0.005 Ω-cm were purchased from Silicon Quest (Santa Clara, CA). Polydimethylsiloxane (PDMS) with curing agent was obtained from Dow Corning (Midland, MI). Phosphate buffered saline (PBS) was obtained from Mediatech (Herndon, VA). Chemicals for microfabrication process were purchased from Honeywell International Inc.

**Liposome preparation.** Fluorescent liposomes consisting of 99% of DOPC (1, 2-dioleoyl-sn-glycero-3-phosphocholine, Avanti) and 1% NBD-PC (1-hexanoyl-2-{6-[(7-nitro-2-1,3-benzoxadiazol-4-yl)amino]hexanoyl}1vc-sn-glycero-3-phosphocholine 810112, Avanti) were prepared by a standard extrusion procedure. The desired composition of the lipids was first mixed in chloroform. The mixture was then dried in a round bottom flask followed by desiccation under nitrogen for at least 30 minutes. Lipid films were then hydrated with 18.2 MΩ-cm deionized (DI) water. The hydrated lipids were extruded through 50 nm and 100 nm pore polycarbonate filters (Whatman, UK) until the suspension reached clarity. The sizes of the liposomes in both deionized (DI) water and PBS were determined by dynamic light scattering. The results are listed in Table S1: Size of liposomes used in the study.

Label	Nanopore size of PC filters (nm)	Diameter (nm)	
		In DI water	In PBS
83 nm	50	86.3±28.1	82.3±29.1
120 nm	100	127.6±38.8	119.9±40.6

**Retention rate determination.** The sample solutions of 83 nm liposomes, 120 nm liposomes, 500nm polystyrene beads, and FITC-BSA were prepared. The sample concentration of both 83 nm and 120 nm liposome are labeled as 150 $\mu$ g lipid/mL. The concentration of 500 nm polystyrene beads is 500  $\mu$ g/mL, and the concentration of FITC-BSA is 50 $\mu$ g/mL. Each sample solution was continuously injected into the prototype through the inlet at a flow rate of 10  $\mu$ L/min by the high precision syringe pump (PHD Ultra Syringe Pump, Harvard Apparatus). The sample was then collected at the outlet in aliquots of 10  $\mu$ L. 8.5  $\mu$ L from each collected sample was mixed with 40  $\mu$ L of water in a 96 well plate and its fluorescent intensity read out by a plate reader (Synergy H4 Hybrid). The concentrations of collected samples were calculated based on the fluorescent intensities. The results were normalized and correlated to sample concentration of the original solution. The retention rates were then determined accordingly.

10

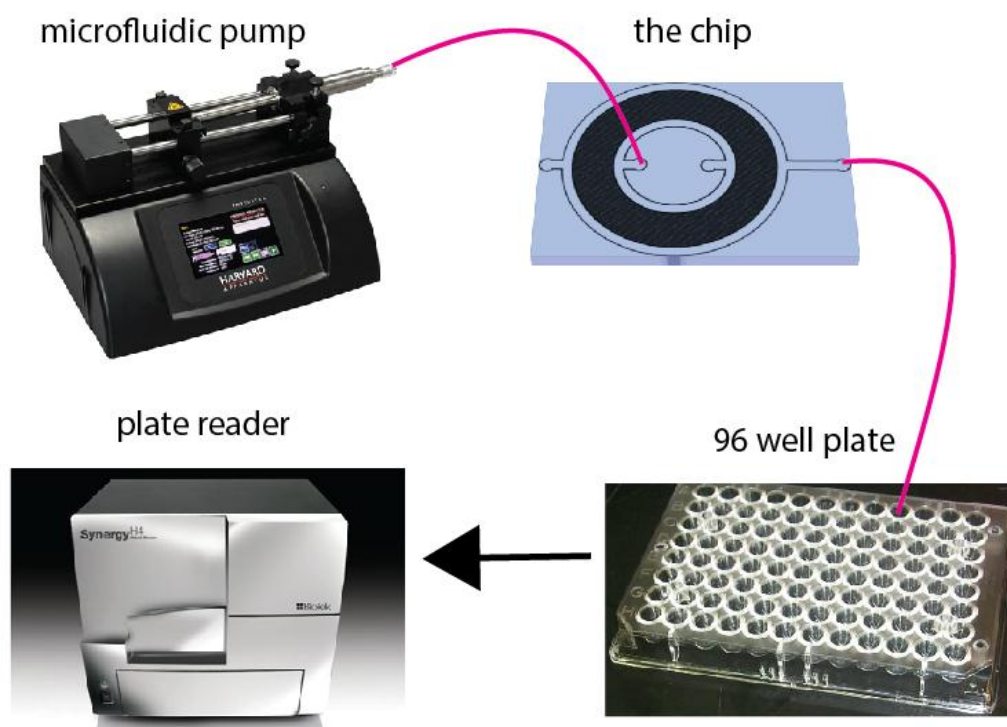


Figure S4. Experimental set-up for retention rate measurement. Microfluidic pump inject fluorescent labeled particles into the device. Samples are collected in a micro-well plate. After dilution, the plate is read out in a plate reader to record the fluorescent intensity. The read out is compared to calibration curves to decide the concentration of particles collected at the outlet of the device.

15